Capped Mohr-Coulomb Plasticity

CSIRO

August 9, 2017

Contents

1 Introduction and the yield functions

Tensile, or Rankine, plasticity is designed to simulate a material that fails when the maximum principal stress exceeds the material's tensile strength. Its yield function is therefore

$$f = \sigma_{\text{max}} - T \, , \tag{1.1}$$

where σ_{max} is the maximum[1] principal stress (the largest eigenvalue of the stress tensor) and T is the tensile strength.

One yield function is sufficient because of the definition $\sigma_{\text{min}} \leq \sigma_{\text{mid}} \leq \sigma_{\text{max}}$. For instance, if during the return-map process both σ_{mid} and σ_{max} exceed T the corresponding admissible configuration is that both of them are equal to T. While one yield function is sufficient, it is convenient to use three yield functions in total:

$$
\begin{aligned}
f_0 &= \sigma_{\text{max}} - T \, , \\
f_1 &= \sigma_{\text{mid}} - T \, , \\
f_2 &= \sigma_{\text{min}} - T \, .
\end{aligned}
\tag{1.2}
$$

This is the version used by `TensileStressUpdate`. These yield functions have been ordered so that the smoothing creates a surface that is perpendicular to the $\sigma_{\text{max}} = \sigma_{\text{mid}}$ plane, and that any trial stress with $\sigma_{\text{mid}} = \sigma_{\text{min}}$ has an admissible returned stress.

Similar remarks hold for compressive plasticity. It yield functions are

$$
\begin{aligned}
f_3 &= -\sigma_{\text{min}} - T_c \, , \\
f_4 &= -\sigma_{\text{mid}} - T_c \, , \\
f_5 &= -\sigma_{\text{max}} - T_c \, .
\end{aligned}
\tag{1.3}
$$

Here T_c is the compressive strength, which is positive for real-world materials, and must always satisfy $T_c > -T$, otherwise there is no admissible region.

Mohr-Coulomb plasticity simulates a material that undergoes shear failure if the shear stress exceeds a linear function of the compressive stress. Its yield functions are

$$
\begin{aligned}
f_6 &= \tfrac{1}{2}(\sigma_{\text{max}} - \sigma_{\text{min}}) + \tfrac{1}{2}(\sigma_{\text{max}} + \sigma_{\text{min}})\sin\phi - C\cos\phi \, , \\
f_7 &= \tfrac{1}{2}(\sigma_{\text{mid}} - \sigma_{\text{min}}) + \tfrac{1}{2}(\sigma_{\text{mid}} + \sigma_{\text{min}})\sin\phi - C\cos\phi \, , \\
f_8 &= \tfrac{1}{2}(\sigma_{\text{max}} - \sigma_{\text{mid}}) + \tfrac{1}{2}(\sigma_{\text{max}} + \sigma_{\text{mid}})\sin\phi - C\cos\phi \, , \\
f_9 &= \tfrac{1}{2}(\sigma_{\text{mid}} - \sigma_{\text{max}}) + \tfrac{1}{2}(\sigma_{\text{mid}} + \sigma_{\text{max}})\sin\phi - C\cos\phi \, , \\
f_{10} &= \tfrac{1}{2}(\sigma_{\text{min}} - \sigma_{\text{mid}}) + \tfrac{1}{2}(\sigma_{\text{min}} + \sigma_{\text{mid}})\sin\phi - C\cos\phi \, , \\
f_{11} &= \tfrac{1}{2}(\sigma_{\text{min}} - \sigma_{\text{max}}) + \tfrac{1}{2}(\sigma_{\text{min}} + \sigma_{\text{max}})\sin\phi - C\cos\phi \, .
\end{aligned}
\tag{1.4}
$$

---

[1] Often the maximum principal stress is denoted by σ_{min}. The code uses the `dsymmetricEigenvalues` method of `RankTwoTensor` and this orders the eigenvalues from smallest to greatest.

Here C is the cohesion and ϕ is the friction angle. Once again, the yield functions have been ordered optimally.

Equations (1.2), (1.3) and (1.4) define the yield functions of Capped Mohr Coulomb plasticity.

The return-map algorithm first rotates σ from the physical frame to the principal-stress frame (where $\sigma = \text{diag}(\sigma_{\min}, \sigma_{\text{mid}}, \sigma_{\max})$). The rotation matrices used are assumed not to change during the return-map process: only $\sigma_{\min}$, σ_{mid} and $\sigma_{\max}$ change. Therefore, at the end of the return-map process these rotation matrices may be used to find the final stress in the physical frame.

The 12 yield functions are smoothed using the method encoded in `MultiParameterPlasticityStressUpdate`. An example is shown Figures 1.1 and 1.2. Figure 1.2 shows slices of the yield surface at various values of the mean stress (that is, on various octahedral planes), and the hexagonal-pyramid and triangular-pyramid nature of the yield surface is evident. The slices taken near the tip and the base highlight: (1) the smoothing; (2) that the smoothing is unsymmetric.

The unsymmetric nature of the yield surface only occurs near the tip and base region where the smoothing mixes the three yield surfaces. For instance, the black line in Figure 1.2 is symmetric, while the red lines are unsymmetric. The amount of asymmetry is small, but it is evident that the red curve is not concentric with the remainder of the curves shown in Figure 1.2. The order of the yield functions in Eqn (1.2), (1.3) and (1.4) have been chosen so that: at the tip the curves intersect the $\sigma_{\max} = \sigma_{\text{mid}}$ line at $90°$, but not on the $\sigma_{\text{mid}} = \sigma_{\min}$ line; at the base the curves intersect the $\sigma_{\text{mid}} = \sigma_{\min}$ line at $90°$, but not on the $\sigma_{\max} = \sigma_{\text{mid}}$ line. The asymmetry does not affect MOOSE's convergence, and of course it is physically irrelevant (since there is no one "correct" smoothed yield surface).
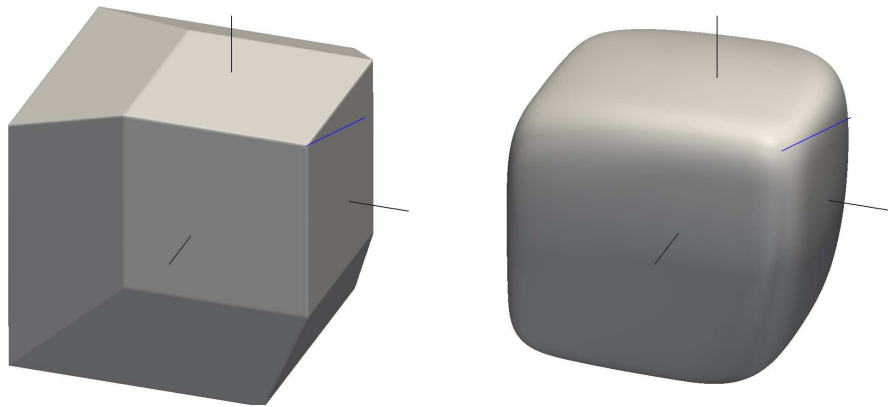

Figure 1.1: Left: the unsmoothed yield surface of capped Mohr-Coulomb plasticity, which is a hexagonal pyramid, capped with a trianglar pyramid at its tip and base (the base is not visible in this picture). Right: a smoothed version. The principal stress directions are shown with black lines, and the mean stress direction is shown with a blue line. In these pictures $C = 3$, $\phi = 30°$, $T = 0.4$, $T_c = 0.7$, and the smoothing solerance is 0.2.
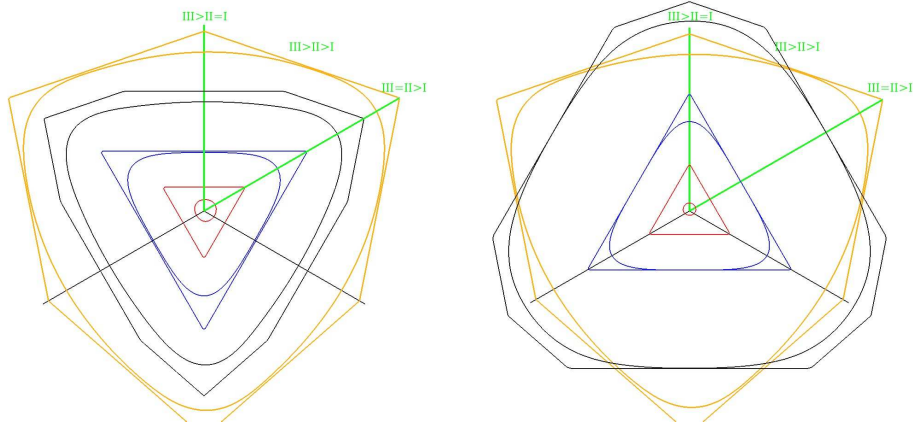
Figure 1.2: Slices of the unsmoothed and smoothed yield functions at various value of mean stress. The viewer is looking along the line of increasing mean stress in these figures. Left: the orange lines show the Mohr-Coulomb hexagon; the black lines show this being truncated by the tensile tip; blue lines show the tensile triangle; red lines show the yield surface near the tip. Right: the similar situation near the compressive base. The whole octahedral plane is shown in this figure, but only one sextant is physical, which is indicated by the solid green lines. In this figure *III* represents σ_{max}, *II* represents σ_{mid} and *I* represents σ_{min}.

2 Flow rules and hardening

The flow potentials for the tensile and compressive parts are associative, while the flow potentials for the Mohr-Coulomb parts are nonassociative. The flow potentials are:

$$
\begin{aligned}
g_0 &= \sigma_{\max} - T \,, \\
g_1 &= \sigma_{\mathrm{mid}} - T \,, \\
g_2 &= \sigma_{\min} - T \,, \\
g_3 &= -\sigma_{\min} - T_c \,, \\
g_4 &= -\sigma_{\mathrm{mid}} - T_c \,, \\
g_5 &= -\sigma_{\max} - T_c \,, \\
g_6 &= \tfrac{1}{2}(\sigma_{\max} - \sigma_{\min}) + \tfrac{1}{2}(\sigma_{\max} + \sigma_{\min})\sin\psi - C\cos\psi \,, \\
g_7 &= \tfrac{1}{2}(\sigma_{\mathrm{mid}} - \sigma_{\min}) + \tfrac{1}{2}(\sigma_{\mathrm{mid}} + \sigma_{\min})\sin\psi - C\cos\psi \,, \\
g_8 &= \tfrac{1}{2}(\sigma_{\max} - \sigma_{\mathrm{mid}}) + \tfrac{1}{2}(\sigma_{\max} + \sigma_{\mathrm{mid}})\sin\psi - C\cos\psi \,, \\
g_9 &= \tfrac{1}{2}(\sigma_{\mathrm{mid}} - \sigma_{\max}) + \tfrac{1}{2}(\sigma_{\mathrm{mid}} + \sigma_{\max})\sin\psi - C\cos\psi \,, \\
g_{10} &= \tfrac{1}{2}(\sigma_{\min} - \sigma_{\mathrm{mid}}) + \tfrac{1}{2}(\sigma_{\min} + \sigma_{\mathrm{mid}})\sin\psi - C\cos\psi \,, \\
g_{11} &= \tfrac{1}{2}(\sigma_{\min} - \sigma_{\max}) + \tfrac{1}{2}(\sigma_{\min} + \sigma_{\max})\sin\psi - C\cos\psi \,.
\end{aligned}
\tag{2.1}
$$

Here ψ is the dilation angle.

The flow rules are

$$
s_a = s_a^{\mathrm{trial}} - \gamma E_{ab}\frac{\partial g}{\partial s_a} \,,
\tag{2.2}
$$

where $s_a = \{\sigma_{\min}, \sigma_{\mathrm{mid}}, \sigma_{\max}\}$ and

$$
E_{ab} = \frac{\partial s_a}{\partial \sigma_{ij}} E_{ijkl} \frac{\partial s_b}{\partial \sigma_{kl}} \,.
\tag{2.3}
$$

In this equation E_{ijkl} is the elasticity tensor.

An assumption that is made in `MultiParameterPlasticityStressUpdate` is that E_{ab} is independent of the stress parameters, s_a and the internal variables. In this case[1]

$$
\frac{\partial s_a}{\partial \sigma_{ij}} = v_i^a v_j^a \,,
\tag{2.4}
$$

where v^a is the eigenvector corresponding to the eigenvalue s^a (of the stress tensor) and there is no sum over a on the right-hand side. Recall that the eigenvectors are fixed during the return-map process, so the RHS is fixed, meaning that E_{ab} is indeed independent of the stress parameters.

---

[1]Special precautions are taken when the eigenvalues are equal, as described in `RankTwoTensor`.

Also recall that the eigenvectors induce a rotation (to the principal-stress frame), so assuming that E_{ijkl} is isotropic

$$E_{ab} = E_{aabb} \, . \tag{2.5}$$

The assumption of isotropy is appropriate for this type of isotropic plasticity.

It is assumed that there are two internal parameters. Note that the definition of internal parameters is motivated by thought experiments or by real experiments, and as such, the following definitions might not suit your needs. It is a small job to produce a new version of `CappedMohrCoulomb` that incorporates different internal parameters.

The "shear" internal parameter is i_0, while the "tensile" internal parameter is i_1. It is assumed that

$$
\begin{aligned}
C &= C(i_0) \, , \\
\phi &= \phi(i_0) \, , \\
\psi &= \psi(i_0) \, , \\
T &= T(i_1) \, , \\
T_c &= T_c(i_1) \, .
\end{aligned}
\tag{2.6}
$$

The evolution of i_0 and i_1 is motivated by first considering a pure shear failure. I would like i_1 to be unchanged in pure shear. A pure shear failure implies

$$
\begin{aligned}
0 &= f = \tfrac{1}{2}(\sigma_{\max} - \sigma_{\min}) + \tfrac{1}{2}(\sigma_{\max} + \sigma_{\min})\sin\phi - C\cos\phi \, , \\
\sigma_{\max} &= \sigma_{\max}^{\mathrm{trial}} - \gamma_{\mathrm{shear}} E_{22}(\tfrac{1}{2} + \tfrac{1}{2}\sin\psi) - \gamma_{\mathrm{shear}} E_{20}(-\tfrac{1}{2} + \tfrac{1}{2}\sin\psi) \, , \\
\sigma_{\min} &= \sigma_{\min}^{\mathrm{trial}} - \gamma_{\mathrm{shear}} E_{00}(-\tfrac{1}{2} + \tfrac{1}{2}\sin\psi) - \gamma_{\mathrm{shear}} E_{02}(\tfrac{1}{2} + \tfrac{1}{2}\sin\psi) \, .
\end{aligned}
\tag{2.7}
$$

The first equation is the yield function and the other equations are the flow rules. Combining the last 2 equations yields

$$\gamma_{\mathrm{shear}} = \frac{(\sigma_{\max}^{\mathrm{trial}} - \sigma_{\min}^{\mathrm{trial}}) - (\sigma_{\max} - \sigma_{\min})}{E_{22} - E_{20}} \tag{2.8}$$

It is assumed that the shear internal parameter evolves according to

$$i_0 = i_0^{\mathrm{old}} + \gamma_{\mathrm{shear}} \, . \tag{2.9}$$

Finally, before considering the tensile failure, note that the equations imply

$$(\sigma_{\max}^{\mathrm{trial}} + \sigma_{\min}^{\mathrm{trial}}) - (\sigma_{\max} + \sigma_{\min}) = \gamma_{\mathrm{shear}}(E_{22} + E_{20})\sin\psi \, . \tag{2.10}$$

Now consider a pure tensile failure. The equations to solve are

$$
\begin{aligned}
0 &= f = \sigma_{\max} - T \, , \\
\sigma_{\max} &= \sigma_{\max}^{\mathrm{trial}} - \gamma_{\mathrm{tensile}} E_{22} \, .
\end{aligned}
\tag{2.11}
$$

The flow rule for $\sigma_{\min}$ is $\sigma_{\min} = \sigma_{\min}^{\mathrm{trial}} - \gamma_{\mathrm{tensile}} E_{20} = \sigma_{\min}^{\mathrm{trial}} - \gamma_{\mathrm{tensile}} \frac{\nu}{1-\nu} E_{22}$, where ν is the Poisson's ratio. Solving these equations yields

$$\gamma_{\mathrm{tensile}} = \frac{\sigma_{\max}^{\mathrm{trial}} - \sigma_{\max}}{E_{22}} = (1 - \nu)\frac{(\sigma_{\max}^{\mathrm{trial}} + \sigma_{\min}^{\mathrm{trial}}) - (\sigma_{\max} + \sigma_{\min})}{E_{22}} \, . \tag{2.12}$$

The final expression is used. To motivate this, consider a pure compressive failure. The equations to solve are

$$0 \;=\; f = -\sigma_{\min} - T_c \;,$$
$$\sigma_{\min} \;=\; \sigma_{\min}^{\text{trial}} + \gamma_{\text{compressive}} E_{00} \;. \qquad (2.13)$$

The flow rule for $\sigma_{\max}$ is $\sigma_{\max} = \sigma_{\max}^{\text{trial}} + \gamma_{\text{compressive}} \frac{\nu}{1-\nu} E_{00}$, where ν is the Poisson's ratio. Solving these equations yields

$$\gamma_{\text{compressive}} = -(1-\nu) \frac{(\sigma_{\max}^{\text{trial}} + \sigma_{\min}^{\text{trial}}) - (\sigma_{\max} + \sigma_{\min})}{E_{00}} \;. \qquad (2.14)$$

Note that $\gamma_{\text{compressive}} = -\gamma_{\text{tensile}}$. This means that when these expressions for the plastic multipliers are used a compressive failure following a tensile failure can cause the tensile internal parameter to reduce, which is physically appealing.

The evolution of the tensile internal parameter is assumed to obey

$$i_1 = i_1^{\text{old}} + (1-\nu) \frac{(\sigma_{\max}^{\text{trial}} + \sigma_{\min}^{\text{trial}}) - (\sigma_{\max} + \sigma_{\min}) - \gamma_{\text{shear}} (E_{22} + E_{20}) \sin \psi}{E_{22}} \;. \qquad (2.15)$$

The reason for the final term involving γ_{shear} is to ensure that no increment of the tensile internal parameter occurs during pure shear failure — see Eqn (2.10). However, the above definitions mean that during pure tensile failure, the shear internal parameter will change.

3 Technical discussions

3.1 Unknowns and the convergence criterion

The return-map problem involves solving the four equations: $f = 0$ (smoothed yield function should be zero) and the flow equations (2.2). The unknowns are the 3 stress parameters $s_a = \{\sigma_{\min}, \sigma_{\mid}, \sigma_{\max}\}$ and the plasticity multiplier γ. Actually, to make the units consistent the algorithm uses γE_{22} instead of simply γ. Convergence is deemed to be achieved when the sum of squares of the residuals of these 4 equations is less than a user-defined tolerance.

3.2 Iterative procedure and initial guesses

A Newton-Raphson process is used, along with a cubic line-search. The process may be initialised with the solution that is correct for perfect plasticity (no hardening) and no smoothing, if the user desires. Smoothing adds nonlinearities, so this initial guess will not always be the exact answer. For hardening, it is not always advantageous to initialise the Newton-Raphson process in this way, as the yield surfaces can move dramatically during the return process.

3.3 Substepping the strain increments

Because of the difficulties encountered during the Newton-Raphson process during rapidly hardening/softening moduli, it is possible to subdivide the applied strain increment, $\delta\varepsilon$, into smaller substeps, and do multiple return-map processes. The final returned configuration may then be dependent on the number of substeps. While this is simply illustrating the non-uniqueness of plasticity problems, in my experience it does adversely affect MOOSE's nonlinear convergence as some Residual calculations will take more substeps than other Residual calculations: in effect this is reducing the accuracy of the Jacobian.

3.4 The consistent tangent operator

MOOSE's Jacobian depends on the derivative

$$H_{ijkl} = \frac{\delta\sigma_{ij}}{\delta\varepsilon_{kl}} \ . \tag{3.1}$$

The quantity H is called the consistent tangent operator. For pure elasticity it is simply the elastic tensor, E, but it is more complicated for plasticity. Note that a small $\delta\varepsilon_{kl}$ simply changes $\delta\sigma^{\text{trial}}$,

so H is capturing the change of the returned stress ($\delta\sigma$) with respect to a change in the trial stress ($\delta\sigma^{\text{trial}}$). In formulae:

$$H_{ijkl} = \frac{\delta\sigma_{ij}}{\delta\sigma_{mn}^{\text{trial}}} \frac{\delta\sigma_{mn}^{\text{trial}}}{\delta\varepsilon_{kl}} = \frac{\delta\sigma_{ij}}{\delta\sigma_{mn}^{\text{trial}}} E_{mnkl} \ . \tag{3.2}$$

In the case at hand,

$$\sigma_{ij} = \sum_a R_{ia} s_a R_{aj}^{\text{T}} \ . \tag{3.3}$$

In this formula σ_{ij} is the returned stress, s_a are the returned stress parameters (eigenvalues), and R is the rotation matrix, defined through the eigenvectors, v^a ($a = 1,2,3$) of the trial stress:

$$R_{ia} = v_i^a \ . \tag{3.4}$$

The three eigenvectors remain unchanged during the return-map process. However, of course they change under a change in σ^{trial}. The relevant formulae are

$$\frac{\delta s_a^{\text{trial}}}{\delta\sigma_{kl}^{\text{trial}}} = v_i^a v_j^a \ , \tag{3.5}$$

$$\frac{\delta v_i^a}{\delta\sigma_{kl}^{\text{trial}}} = \sum_{b \neq a} \frac{v_i^b (v_k^b v_l^a + v_l^b v_k^a)}{2(s_a - s_b)} \ . \tag{3.6}$$

On the RHS of these equations there is no sum over a.

The final piece of information is

$$\frac{\delta s_b}{\delta s_a^{\text{trial}}} \ . \tag{3.7}$$

`MultiParameterPlasticityStressUpdate` computes this after each Newton step, for any aribtrary plasticity model.

The nontrivial part to the consistent tangent operator is therefore

$$\frac{\delta\sigma_{ij}}{\delta\sigma_{mn}^{\text{trial}}} = \sum_a \frac{\delta R_{ia}}{\delta\sigma_{mn}^{\text{trial}}} s_a R_{aj}^{\text{T}} + \sum_a \sum_b R_{ia} \frac{\delta s_a}{\delta s_b^{\text{trial}}} \frac{\delta s_b^{\text{trial}}}{\delta\sigma_{mn}^{\text{trial}}} R_{aj}^{\text{T}} + \sum_a R_{ia} s_a \frac{\delta R_{aj}^{\text{T}}}{\delta\sigma_{mn}^{\text{trial}}} \ . \tag{3.8}$$

All the components of this equation have been provided above.

3.5 Cosserat version

A Cosserat version of capped Mohr-Coulomb plasticity is available. It assumes a "host" non-Cosserat isotropic elasticity tensor exists, and this is employed in the return-map algorithm. The unsymmetric parts of the stress tensor and the moment-stress tensor do not enter into the plasticity theory, so they are unaffected during plastic deformation.

4 Tests

The test suite consists of many tests of `CappedMohrCoulombStressUpdate`. This Chapter describes a few of these.

4.1 The tensile yield surface

Consider the tip of the tensile yield surface shown in Figure 4.1. Repeated deformations may be applied to a single element in order to cause tensile failure, and by recording the returned stresses, the yield surface may be mapped out. Figure 4.1 shows that MOOSE produces the expected result. The tests are `small_deform5`, `small_deform6` and `small_deform7`.
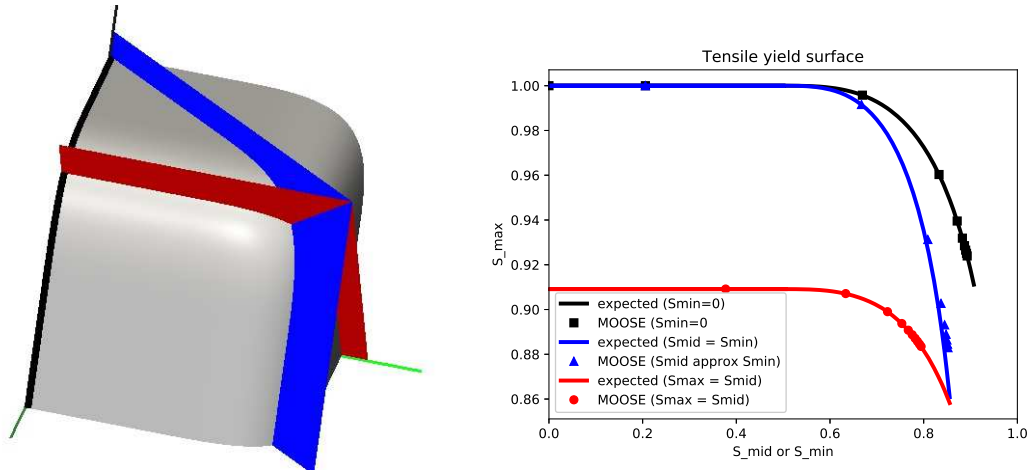

Figure 4.1: The tip of the tensile yield surface. This surface has $T = 1$ and the smoothing parameter is 0.5. The principal stress axes are shown in black (σ_{max}), dark green (σ_{mid}) and light green (σ_{min}). The wedge-shaped region defined by the planes is the physical region where $\sigma_{max} \geq \sigma_{mid} \geq \sigma_{min}$. The blue plane is $\sigma_{mid} = \sigma_{min}$, which is a Lode angle of $-30°$. The red plane is $\sigma_{max} = \sigma_{mid}$, which is a Lode angle of $30°$. The black curve has $\sigma_{min} = 0$. The right figure shows plots of the yield surface along these curves (with the same colour scheme) demonstrating that MOOSE produces the expected result. There is a tiny discrepancy in the blue ($\sigma_{mid} = \sigma_{min}$) result: this is because the deformations applied in the test only produce the approximate result $\sigma_{mid} \approx \sigma_{min}$, so the MOOSE results don't lie exactly on the blue plane, but slightly off it.

4.2 The compressive yield surface

Consider the tip of the compressive yield surface shown in Figure 4.2. Repeated deformations may be applied to a single element in order to cause compressive failure, and by recording the returned stresses, the yield surface may be mapped out. Figure 4.2 shows that MOOSE produces the expected result. The tests are `small_deform15`, `small_deform16` and `small_deform17`.
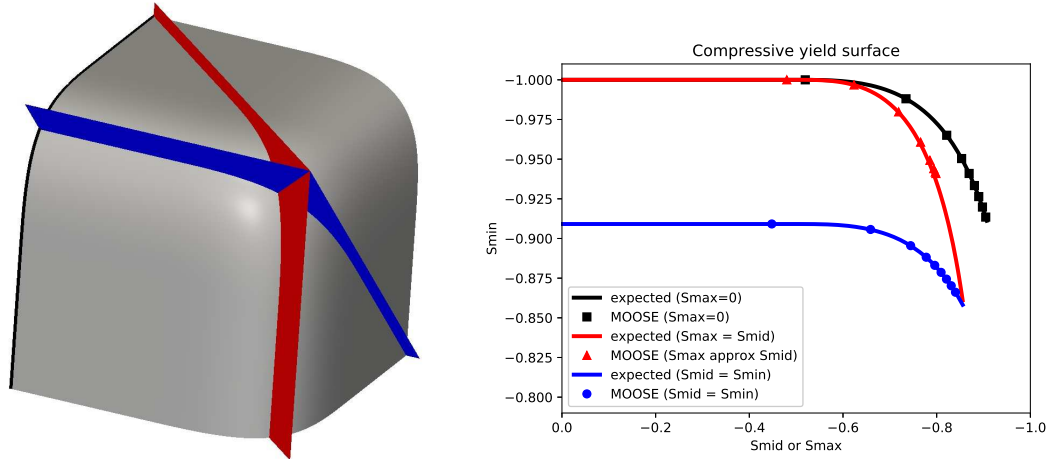

Figure 4.2: The tip of the compressive yield surface (this view has opposite orientation to Figure 4.2). This surface has $T_c = 1$ and the smoothing parameter is 0.5. The wedge-shaped region defined by the planes is the physical region where $\sigma_{max} \geq \sigma_{mid} \geq \sigma_{min}$. The blue plane is $\sigma_{mid} = \sigma_{min}$, which is a Lode angle of $-30°$. The red plane is $\sigma_{max} = \sigma_{mid}$, which is a Lode angle of $30°$. The black curve has $\sigma_{max} = 0$. The right figure shows plots of the yield surface along these curves (with the same colour scheme) demonstrating that MOOSE produces the expected result. There is a tiny discrepancy in the red ($\sigma_{max} = \sigma_{mid}$) result: this is because the deformations applied in the test only produce the approximate result $\sigma_{max} \approx \sigma_{mid}$, so the MOOSE results don't lie exactly on the blue plane, but slightly off it.

4.3 The Mohr-Coulomb yield surface on the octahedral plane

Consider the slice of the Mohr-Coulomb yield surface shown in Figure 4.3, where the mean stress is zero: $\mathrm{Tr}\,\sigma = 0$. Repeated deformations may be applied to a single element in order to cause shear failure, and by recording the returned stresses, the yield surface may be mapped out. The result is shown in Figure 4.3. The test is `small_deform21`.
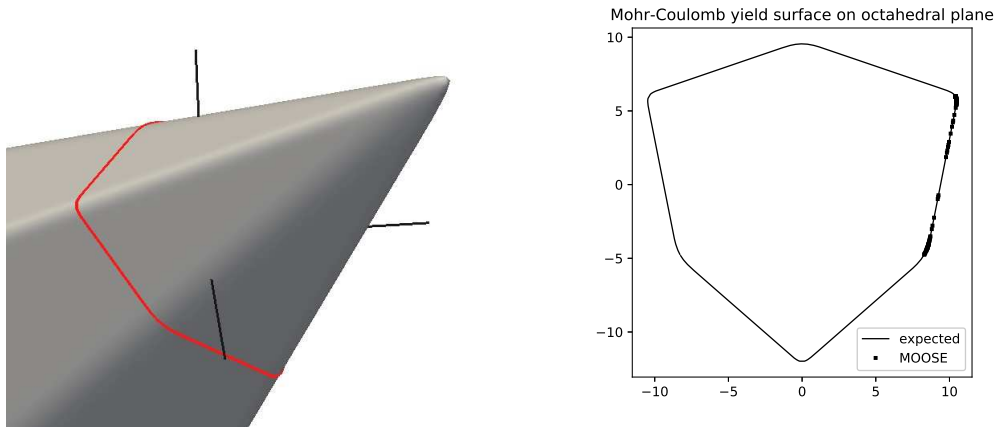
Figure 4.3: Left: The tip of the Mohr-Coulomb yield surface. This surface has $C = 10$, $\phi = 20°$, and is smoothed with a smoothing parameter of 1.0. The principal stress axes are shown in black. The octahedral plane, where the mean stress is zero ($\mathrm{Tr}\,\sigma = 0$) is represented by the red line around the yield surface. Right: The expected result is the hexagon, and the MOOSE results lie on the hexagon as desired. Only the physical sextant ($\sigma_{\mathrm{max}} \geq \sigma_{\mathrm{mid}} \geq \sigma_{\mathrm{min}}$) is sampled by MOOSE.

4.4 The Mohr-Coulomb yield surface on the meridional plane

Consider the two slices of the Mohr-Coulomb yield surface[1] that are shown in Figure 4.4. Repeated deformations may be applied to a single element in order to cause shear failure, and by recording the returned stresses, the yield surface may be mapped out. Figure 4.4 shows the results on the two meridional planes, indicating that MOOSE's Mohr-Coulomb yield functions are coded correctly. The tests are `small_deform23` and `small_deform24`.

Looking carefully at the smoothed tip in Figure 4.4, the effect of the ordering of the yield functions is evident: the lines do not intersect the mean stress axis at precisely $90°$. Nevertheless, the yield surface is provably convex, and the non-right intersection means that MOOSE will stay away from the numerically troublesome regions such as $\sigma_{\mathrm{max}} = \sigma_{\mathrm{mid}} = \sigma_{\mathrm{min}}$.

4.5 Hardening of the tensile and compressive strengths

Both the tensile strength and the compressive strength may depend on the internal parameter i_1. Example cubic relationships are shown in Figure 4.5. The tests are `small_deform_hard3` and `small_deform_hard13`.

---

[1]An unusually large amount of smoothing has been used in this figure: I suggest in real situations the smoothing parameter be approximately $C/10$.
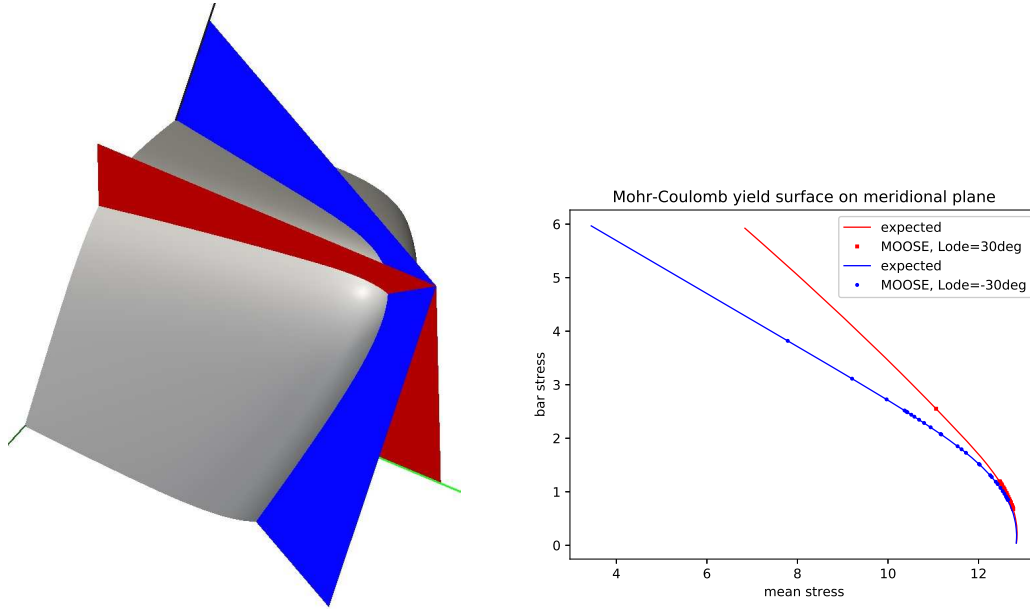
Figure 4.4: Left: The tip of the Mohr-Coulomb yield surface. This surface has $C = 10$, $\phi = 30°$, and is smoothed with a smoothing parameter of 5.0. The principal stress axes are shown in black (σ_{max}), dark green (σ_{mid}) and light green (σ_{min}). The wedge-shaped region defined by the planes is the physical region where $\sigma_{max} \geq \sigma_{mid} \geq \sigma_{min}$. The blue plane is $\sigma_{mid} = \sigma_{min}$, which is a Lode angle of $-30°$. The red plane is $\sigma_{max} = \sigma_{mid}$, which is a Lode angle of $30°$. Right: The Mohr-Coulomb yield surface on the two meriodonal planes (blue and red). The MOOSE results are shown as blue and red spots. The axes are mean stress $= \mathrm{Tr}\,\sigma/3$ and bar stress $= \sqrt{s_{ij}s_{ij}/2}$, where s_{ij} is the deviatoric part of the stress tensor.

4.6 Hardening of the cohesion and friction angle

Both the cohesion and friction angle may depend on the internal parameter i_0. Example cubic relationships are shown in Figure 4.6. The tests are small_deform_hard21 and small_deform_hard22.

4.7 Return to the yield surface from random positions

Random displacements may be applied to a mesh in order to cause failure in the elements, and the returned stresses may be recorded. The test is random5. The results are shown in Figure 4.7 where it is clear that MOOSE returns correctly to the yield surface.
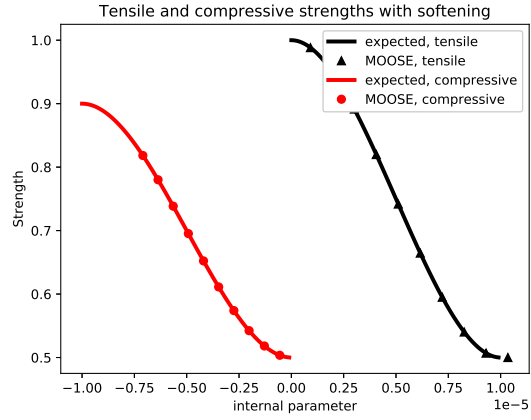
14

Figure 4.5: Examples of hardening of the tensile and compressive strengths, demonstrating that MOOSE produces the expected behaviour.
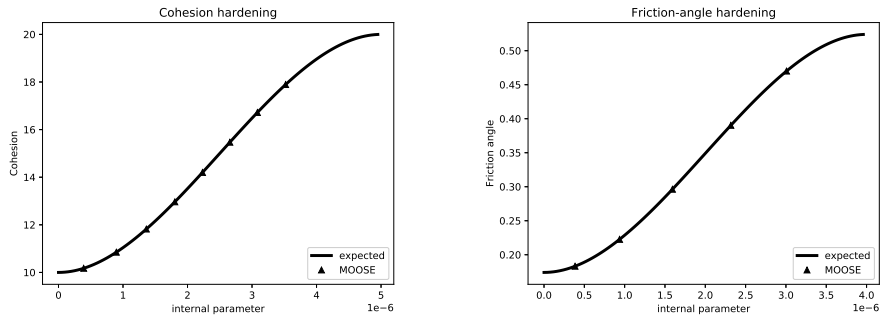

Figure 4.6: Examples of hardening of the cohesion and friction angle, demonstrating that MOOSE produces the expected behaviour.
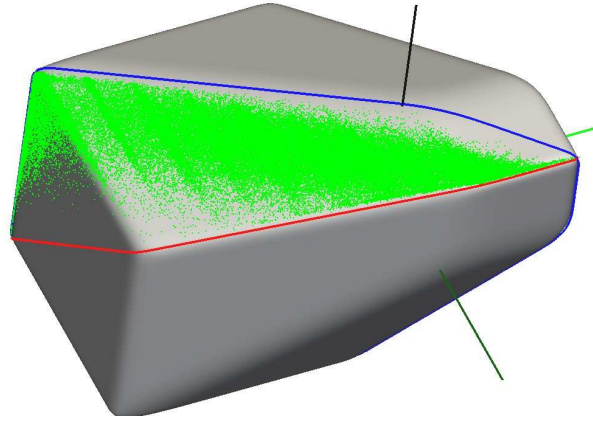
Figure 4.7: Grey shape: the capped Mohr-Coulomb yield surface with $T = 1.5$, $T_c = 3$, $C = 1$, $\phi = 20°$ and smoothing parameter of 0.2. The other parameters are $\psi = 3°$ and Poisson's ratio $\nu = 0.3$. The principal stress axes are shown in black (σ_{max}), dark green (σ_{mid}) and light green (σ_{min}). The plane defined by the red curve has $\sigma_{max} = \sigma_{mid}$ (Lode angle of $30°$), and the plane defined by the blue curve has $\sigma_{mid} = \sigma_{min}$ (Lode angle of $-30°$. The physical region is the sextant lying between these curves. Upon randomly deforming a mesh, the stresses in each element that experiences plastic deformation will lie on the yield surface. The green dots are the results from 123400 applications of the return-map algorithm. They lie on the yield surface as desired.